Published in final edited form as:
J Mol Biol. 2007 September 21; 372(3): 649–659.

Crystal structure of the *Escherichia coli* regulator of σ^{70}, Rsd, in complex with σ^{70} domain 4

Georgia A. Patikoglou[*], **Lars F. Westblade**[*], **Elizabeth A. Campbell**, **Valérie Lamour**, **William J. Lane**, and **Seth A. Darst**
The Rockefeller University, Box 224, 1230 York Avenue, New York, NY 10021, USA.

Summary

The *Escherichia coli* Rsd protein binds tightly and specifically to the RNA polymerase (RNAP) σ^{70} factor. Rsd plays a role in alternative σ factor-dependent transcription by biasing the competition between σ^{70} and alternative σ factors for the available core RNAP. Here, we determined the 2.6 Å-resolution X-ray crystal structure of Rsd bound to σ^{70} domain 4 (σ^{70}_4), the primary determinant for Rsd binding within σ^{70}. The structure reveals that Rsd binding interferes with the two primary functions of σ^{70}_4, core RNAP binding and promoter –35 element binding. Interestingly, the most highly conserved Rsd residues form a network of interactions through the middle of the Rsd structure that connect the σ^{70}_4-binding surface with three cavities exposed on distant surfaces of Rsd, suggesting functional coupling between σ^{70}_4 binding and other binding surfaces of Rsd, either for other proteins or for as yet unknown small molecule effectors. These results provide a structural basis for understanding the role of Rsd, as well as its ortholog, AlgQ, a positive regulator of *Pseudomonas aeruginosa* virulence, in transcription regulation.

Keywords

RNA; polymerase/Rsd/Sigma; factor/Transcription; regulation/X-ray; crystallography

Introduction

In bacteria, the 450 kDa RNA polymerase (RNAP) holoenzyme, comprising the evolutionarily conserved catalytic core (subunit composition $\alpha_2\beta\beta'\omega$) combined with the initiation-specific σ subunit, directs transcription initiation [1]. The principal control point of gene expression in bacteria is transcription initiation, and a major mechanism by which bacteria regulate transcription initiation is through regulation of σ activity [2]. The activity of most σ factors is determined by their cellular level, their affinity for RNAP, and their interactions with regulatory proteins that bind and modulate σ factor function.

In *Escherichia coli* (*Ec*), the primary σ factor, σ^{70}, has the highest affinity for core RNAP and is also the most abundant σ factor throughout the growth cycle [3; 4]. Thus, it is not clear how alternative σ factors capture sufficient core RNAP to express genes under their control. The discovery of the σ^{70}-binding protein Rsd provided a partial solution to this problem [5].

Dr. Darst: phone, 212-327-7479; FAX, 212-327-7477; e-mail, darst@rockefeller.edu.
[*]both of these authors contributed equally to this work

Biochemical and genetic studies demonstrated that Rsd can indirectly stimulate transcription from alternative σ factor-dependent promoters by binding to σ^{70} with a stoichiometry of 1:1 [5–10]. Mapping of the primary Rsd-binding determinant on σ^{70} was localized to σ^{70} domain 4 (σ^{70}_4; [10–12], a structural domain of σ^{70} that binds the RNAP β-subunit flap-tip, recognizes the –35 promoter element, and is a target for many transcriptional activators) [13–17].

The amino acid sequence of Rsd is 55% similar to the sequence of the *Pseudomonas aeruginosa* (*Paer*) AlgQ transcription regulator. *Paer* is an opportunistic pathogen and causative agent of microbial corrosion. AlgQ is important in regulating the production of alginate, neuraminidase, and pyoverdine; factors that are necessary for promoting *Paer* virulence [18–22]. *Ec* Rsd can complement AlgQ in the production of pyoverdine [18]. Thus, it has been proposed that *Paer* AlgQ binds to and modulates the activity of *Paer* σ^{70} in a manner similar to *Ec* Rsd [11; 18].

Here, we describe the 2.6 Å-resolution X-ray crystal structure of the *Ec* σ^{70}_4/Rsd complex. The results provide a structural basis for future experiments addressing the role of both Rsd and AlgQ in regulating σ activity.

Results

Crystallization, structure determination, and overall structure of the σ^{70}_4/Rsd complex

Rsd appears to interact with *Ec* σ^{70} primarily through determinants within σ^{70}_4 [10–12]. Although *Ec* σ^{70}_4 on its own is poorly behaved for structural studies [23], co-expression of *Ec* σ^{70}_4 (*Ec* σ^{70} residues 541–613) with Rsd resulted in a soluble complex that was purified to homogeneity with high yield (Materials and Methods). Alongside the *Ec* σ^{70}_4/Rsd complex, *Paer* AlgQ and *Paer* σ^{70}_4 were co-expressed and purification of the complex attempted. Although there is evidence that the proteins interact (Ref. 11; L.F.W. and S.A.D., unpublished), the complex of *Paer* proteins was unstable and did not survive the purification procedure (data not shown).

Rod-like crystals with approximate dimensions of 180 × 20 × 20 μm, space group $p6_4$ (a = b = 84.111 Å, c = 84.219 Å), were grown using vapor diffusion (Materials and Methods). The crystals contained one 26.7 kDa σ^{70}_4/Rsd complex per asymmetric unit, with a solvent content of 64%. The crystals diffracted isotropically to 2.6 Å-resolution. The structure of the complex was solved by Multiwavelength Anomalous Diffraction [24] using data from selenomethionyl-substituted protein crystals (Table 1; Figure S1). Cycles of iterative model building and crystallographic refinement converged to an R/R_{free} of 0.239/0.267 at 2.6 Å-resolution (Table 1).

The structure reveals a σ^{70}_4/Rsd complex with a stoichiometry of 1:1 (Figure 1). This is consistent with the gel filtration behavior of the σ^{70}_4/Rsd complex during purification (data not shown), and with previous biochemical experiments indicating a 1:1 stoichiometry of the full-length σ^{70}/Rsd complex in solution [10].

Rsd structure

The Rsd structure comprises four core α-helices (helices H2–H5; Figure 1) packed in an up-and-down bundle with a slight left-handed twist. An additional short N-terminal α-helix (H1) is tucked against the side of the bundle against H2 and H5. The Rsd fold is remarkably similar to the vinculin tail domain. Superposition of Rsd with the vinculin tail domain (chicken vinculin residues 901–1046; Ref. 25) over the entire length of Rsd (residues 1–153) but excluding exposed loops connecting the α-helices yields a root-mean-square deviation of 2.53 Å over 116 α-carbons (Figure S2). Rsd therefore belongs to the vinculin/α-catenin superfamily of proteins [26]. Vinculin and α-catenin are structural components of the eukaryotic cytoskeleton,

while Rsd is a bacterial transcriptional regulator. At this point we do not believe there is any functional significance to the observed structural similarity.

A distinctive structural feature of Rsd is a pronounced kink (~30°) in H3. The kink occurs around a highly conserved Gly residue at position 68 (Figure 1). In an alignment of 113 Rsd orthologs (Supplemental Information), Gly occurs at this position in 110 of the sequences (97% identity, Figure 2). Moreover, the primary Rsd binding interface with σ^{70}_4 is centered at the kink (Figure 1). All of the absolutely conserved Rsd residues that contact σ^{70}_4 lie near the H3 kink (Asp63, Ser66, Phe70; Figures 2 and 3). These observations suggest that the kink is a conserved feature of the Rsd structure that is important for σ^{70}_4 binding.

Interactions between σ^{70}_4 and Rsd

Binding of σ^{70}_4 to Rsd buries a modest 779 $Å^2$ of protein surface area. Nevertheless, the protein/protein complex is very stable, as it survives several purification steps without dissociating. All of the interactions between σ^{70}_4 and Rsd are schematically diagrammed in Figure 3A, and a stereo view of the interface with the involved amino acids is shown in Figure 3B.

The σ^{70}_4/Rsd interface, centered about the kink in Rsd-H3, involves hydrophobic interactions with a patch of highly conserved residues from H3 exposed on the surface of Rsd (Figure 3). Rsd residues Val62 and Leu65 are conserved as hydrophobic residues, while Ser66 (which makes van der Waals contacts through its β-carbon), Ala67, and Phe70 are absolutely conserved (Figure 2). The interface includes polar interactions involving mostly residues from Rsd-H4. The protein/protein interaction is also stabilized by two salt bridges between pairs of highly conserved, oppositely-charged residues (σ^{70}_4-Arg562/Rsd-Asp63; σ^{70}_4-Arg596/Rsd-Asp108).

The structural observations are completely consistent with biochemical and genetic studies on the σ^{70}_4/Rsd interaction. Previous studies implicated σ^{70}_4 region 4.2 as the primary determinant in the σ^{70}/Rsd interaction [10–12], which is borne out by the structure (Figure 3A). Detailed genetic studies have implicated residues in σ^{70}_4 that the structure shows are involved in, or are near, the σ^{70}_4/Rsd interface (σ^{70}_4-590/591/593/595/596/598; [10–12]. A more recent study showed that mutation of Rsd-Asp63 (involved in a conserved salt bridge with σ^{70}_4-Arg562) to Ala caused a severe defect in Rsd binding to σ^{70} [9].

Conserved residues in Rsd form an interacting network

The alignment of Rsd orthologs (Supplementary information) reveals 13 absolutely conserved residues distributed throughout helices H2–H5 (4 conserved residues in H2, 5 in H3, 1 in H4, 3 in H5; red bars in histogram of Figure 2). Only three of the absolutely conserved residues, all on H3, contact σ^{70}_4 (Rsd Asp63, Ser66, and Phe70; Figure 2). Remarkably, all 13 absolutely conserved residues form an interacting network that extends through the middle of the Rsd structure (Figure 4). The interacting network includes both polar (green lines in Figure 4B) and van der Waals (orange lines, Figure 4B) interactions. The network links the σ^{70}_4 binding surface with three exposed cavities on the Rsd surface (labelled I, II, and III in Figure 4).

Taking the σ^{70}_4 binding surface of Rsd as the front, Cavity I is located on the side of the molecule and is lined with conserved residues Asp20 and Leu23 (Figure 4). Cavity II is located on the back of Rsd and is lined with conserved residues Arg26 and Asp142. Most interesting is Cavity III, a deep (approximately 8 Å), narrow (approximately 3 Å in diameter) ‘hole’ penetrating into the structure between H2 and H3. Cavity III is large enough to accommodate a water molecule. Cavity III is lined by conserved residues Trp22, Tyr64, Arg137, and Glu141. Most of the surface of Cavity III is lined with polar atoms (Trp22 NE1; Tyr64 O; Leu65 O; Gly68 N; Tyr73 OH; Arg137 NH1; Glu141 OE2), but one surface comprises the hydrophobic

face of the aromatic ring of Tyr64. Note that conserved residues Arg137 and Glu141, which form a salt bridge (Arg137 NH1–Glu141 OE2 distance = 3.62 Å), are completely buried in the interior of the Rsd structure except for the exposure of Arg137 NH1 and Glu141 OE2 on the solvent-accessible surface of Cavity III.

Ecσ^{70}_4 structure and the relationship of Rsd with T4 AsiA

Structures of σ_4 from σ^{70}-family members have been observed individually (*Thermus aquaticus* [*Taq*] σ^{A}_4; Ref. 13), in complex with –35 element promoter DNA (*Taq* σA_4; Ref. 13), in complex with anti-σ factors (*Ec* σ^{E}_4; Ref. 27; *Aquifex aeolicus* σ^{28}_4; Ref. 28), and in complex with core RNAP (*Taq* σ^{A}_4; Ref. 16; *Thermus thermophilus* σ^{A}_4; Ref. 17). In all of these cases mentioned above, the σ_4 domain comprises a compact structural core of three α-helices (corresponding to residues 551–599 of *Ec* σ^{70}_4) that is essentially identical in all of the structures. The last two α-helices of the structural core make up the helix-turn-helix motif that is responsible for recognition of the promoter –35 element [13]. In one case, however, the interaction of *Ec* σ^{70}_4 with the anti-σ and appropriator AsiA from bacteriophage T4 induces a dramatic structural rearrangement of σ^{70}_4 [29].

In the σ^{70}_4/Rsd complex, the structure of *Ec* σ^{70}_4 is nearly identical to the undistorted σ_4 structures that have been observed previously. For instance, superimposing the 49-residue structural core of *Ec* σ^{70}_4 (residues 551–599) from the σ^{70}_4/Rsd complex with *Taq* σ^{A}_4 (PDB ID 1KU3, residues 376–424; Ref. 13) results in an rmsd in α-carbon positions of 1.6 Å (Figure S3). Regions to the N- and C-terminus of the structural core deviate in structure, but these regions are known to be structurally variable depending on the functional context [13].

Pineda et al.[30] proposed that the T4-type phage AsiA orthologs and Rsd orthologs are members of a related family that interact similarly with their cognate σ factors. Although Jishage & Ishihama [5] concluded in their analysis that there was no significant sequence similarity between Rsd and T4 AsiA, Pineda et al. [30] present an alignment between T4-type phage AsiA orthologs and the N-terminal 82 residues of Rsd and suggest that it indicates significant similiarity. However, the Pinda et al. [30] alignment between T4-phage AsiA and Rsd[1–82] contains many gaps for such a short segment, and despite this the sequence identity between T4-phage AsiA and Rsd is only about 7% (6 out of 82 Rsd residues), which is similar to the sequence identity expected for the alignment of completely random sequences (6%). Indeed, structural comparison of T4 AsiA [31] and Rsd does not support the idea that these proteins belong to a related family of proteins (Figure S4). Moreover, T4 AsiA dramatically distorts the σ^{70}_4 structure [29], while Rsd does not.

Rsd binding to σ^{70}_4 occludes both RNAP and promoter DNA binding by σ^{70}_4

In the RNAP holoenzyme, σ_4 interacts with the core RNAP by binding to the RNAP β-subunit flap-tip-helix [14–17]. Analysis of the σ^{70}_4/Rsd complex predicts that Rsd would sterically interfere with the binding of σ^{70}_4 to the β-flap-tip-helix (Figure 5). Rsd also directly interacts with several σ^{70}_4 residues that interact with the β-flap-tip in the RNAP holoenzyme (σ^{70}_4-Phe563, Leu595, and Arg599). Indeed, a core RNAP binding defect results from mutation of σ^{70}_4-Phe563 [32; 33].

In the RNAP holoenzyme open promoter complex, in addition to the β-flap-tip helix, σ^{70}_4 also binds the promoter DNA –35 element. Analysis of the σ^{70}_4/Rsd complex predicts that Rsd would sterically interfere with the binding of σ^{70}_4 to the –35 element DNA (Figure 5). Rsd also directly interacts with several σ^{70}_4 residues that interact with the promoter DNA (σ^{70}_4-Arg562, Leu573, Arg584, and Arg588; Ref. 13). Both σ^{70}_4-Arg584 and Arg588 have been shown to be important for sequence-specific recognition of the –35 element [34; 35; 36]. We

conclude that σ^{70}_4 bound to Rsd would not be able to interact with the RNAP β-flap-tip nor would it be able to interact with the promoter –35 element.

Conclusions

Rsd was identified on the basis of its tight binding to *Ec* σ^{70} [5]. The binding is specific for σ^{70}, as Rsd does not associate with alternative σ factors [5]. Data are consistent with Rsd playing a role in assisting alternative σ factor-dependent transcription by biasing the competition between σ^{70} and alternative σ factors for the available core RNAP through its interaction with σ^{70} [6–9].

The structure of Rsd bound to σ^{70}_4, the primary determinant for Rsd binding within σ^{70} [10–12], reveals that Rsd binding interferes with the two primary functions of σ_4, core RNAP binding and promoter –35 element binding (Figure 5). Interestingly, the most highly conserved residues of Rsd form a network of interactions through the middle of the Rsd structure that connect the σ^{70}_4-binding surface with three cavities exposed on distant surfaces of Rsd. This suggests functional coupling between σ^{70}_4 binding and other binding surfaces of Rsd, either for other proteins or for as yet unkown small molecule effectors. Rsd is known to participate in protein/protein interactions in addition to the one with σ^{70}_4, including with the core RNAP [37; 38], and with other σ^{70} domains (L.F.W. and S.A.D., unpublished). The possibility that Rsd may interact with small molecule effectors, particularly through Cavity III (Figure 4), which does not seem appropriate for a protein/protein interaction, has not, to our knowledge, been considered previously. The identification of a putative small molecule ligand for Rsd could greatly facilitate the understanding of Rsd's role in the regulation of transcription. Finally, due to the high sequence similarity between σ^{70}_4 from *Ec* and *Paer*, and between *Ec* Rsd and *Paer* AlgQ, the structure of the *Ec* σ^{70}_4/Rsd complex provides a structural basis for understanding the mechanism of action of AlgQ, a global regulator of virulence in the pathogen *Paer*.

Materials and Methods

Construction of the *Ec*σ^{70}_4/Rsd co-expression cassette

The *Ec* σ^{70}_4/Rsd co-expression plasmid was constructed in three steps based upon the procedure of [39]. First, DNA encoding full-length Rsd (residues 1–158) was amplified by the polymerase chain reaction (PCR), digested with NdeI and BamHI restriction endonucleases, and cloned between the NdeI and BamHI sites of pET21a (Novagen) generating pET21aRsd. Second, DNA encoding *Ec* σ^{70}_4 (*Ec* σ^{70} residues 541–613) was amplified by PCR, cleaved with NdeI and HindIII, and cloned between the NdeI and HindIII sites of a pET28a-based plasmid, creating pSKB2*Ec*σ^{70}_4. Finally, using pSKB2*Ec*σ^{70}_4 as a template, the DNA encoding the pET28a-based translation initiation regions and the coding sequence of *Ec* σ^{70}_4 was amplified by PCR, cleaved with BamHI and HindIII, and cloned between the BamHI and HindIII sites of pET21aRsd, creating pET21aRsd/*Ec*σ^{70}_4.

Expression and Purification of the *Ec*σ^{70}_4/Rsd complex

The expression plasmid pET21aRsd/*Ec*σ^{70}_4 was transformed into BL21 (DE3) *Ec* cells and transformants were selected in the presence of the appropriate antibiotic. Cultures were grown at 37 °C to an A600 nm ~0.6 and induced with 1 mM IPTG for 3 hours at 30°C. Cells containing overexpressed proteins were harvested by centrifugation and stored at minus 80°C.

The *Ec* σ^{70}_4/Rsd complex (*Ec* σ^{70}_4 contains an N-terminal His_6-tag and PreScission cleavage site derived from the vector) was purified by HiTrap Ni^{2+}-charged affinity chromatography (GE Healthcare), and the N-terminal His_6-tag was removed using PreScission protease (GE

Healthcare). The sample was further purified by a second, subtractive HiTrap Ni^{2+}-charged affinity chromatography step to remove uncleaved His_6-σ^{70}_4 protein and the His_6-tag, ion exchange chromatography (HiTrap Q Sepharose; GE Healthcare) and gel filtration chromatography (Superdex 75; GE Healthcare). Purified σ^{70}_4/Rsd complex was concentrated to ~16 mg/ml using centrifugal filtration units (Vivascience) and exchanged into buffer containing 10 mM Tris-HCl (pH 8.0), 0.2 M NaCl, 5 mM DTT. Selenomethionyl-substituted complex was prepared for MAD analysis by suppression of methionine biosynthesis [40], and purified using similar procedures.

Crystallization and Structure Determination

Rod-like crystals were initially obtained by vapour diffusion using a sitting drop setup in 96-well plates using a sparse matrix screen (Hampton Research) at 4°C by mixing 1 μL of protein solution with 1 μL of well solution (0.2 M KCl, 0.05 M $MgCl_2$, 0.05 M Tris-HCl, pH 7.5, 10% PEG4000) and equilibrating against 100 μL of well solution. Attempts to reproduce the original crystallization condition in a larger 24-well plate using a hanging drop vapour diffusion setup and a grid screen around the original condition yielded needle-like crystals. Crystal growth was optimized using a combination of grid screening and microseeding using Seed Beads (Hampton Research).

Crystals were prepared for cryocrystallography by incubating in cryosolution (0.2 M KCl, 0.05 M $MgCl_2$, 0.05 M Tris-HCl, pH 7.5, 10% PEG4000, 25% glycerol) for 1 minute. The crystals were then flash frozen in a vial of liquid nitrogen and stored at liquid nitrogen temperature. MAD data were collected from the crystals of selnomethioyl-substituted complex at two wavelengths corresponding to the peak and one remote value of the X-ray absorption spectrum (λ1 and λ2, respectively, Table 1).

Four Se sites (out of a possible six Se sites) were located using SnB [41] with the anomalous signal from the SeMet(λ1) dataset. Phases were calculated using SHARP [42]. The experimental electron density map, after density modification using SOLOMON [43], was excellent (Figure S1). Model building was performed manually using O [44]. Iterative model building and refinement against the native amplitudes were performed using CNS [45]. The final model contains Rsd residues 1–42 and 50–158 (the loop region 43–49 is disordered), *Ec* σ^{70}_4 residues 546–613, one Mg^{2+}-ion, and 98 water molecules. Analysis of the structure using PROCHECK [46] showed 91% of the residues in the most favored regions of the Ramachandran plot, and 9% in additional allowed regions (no residues in generously allowed or disallowed regions), and an overall G factor of 0.3.

Sequence alignment

The sequence alignment of 113 Rsd orthologs (Supplemental information) was generated by using the *Ec* K-12 Rsd sequence to BLAST the NCBI non-redundant database, followed by sequence retrieval. The downloaded sequences, which included both Rsd and *Paer* AlgQ, were then aligned using PCMA (ftp://iole.swmed.edu/pub/PCMA/) (PMID: 12584134).

Accession codes

The coordinates for the refined σ^{70}_4/Rsd structure have been deposited in the Protein Data Bank (accession code 2P7V).

Supplementary Material

Refer to Web version on PubMed Central for supplementary material.

Acknowledgements

We are indebted to Stephen K. Burley, Stephen Busby, Ann Hochschild, Annie Kolb, Ivo Lorenz, Joseph Marcotrigiano, Bryce Nickels, and Andy Yuan for helpful discussions. We thank Stephen R. Wasserman (SGX-CAT) and Howard Robinson (NSLS X29) for support at the synchrotron facilities. Financial support for beamline X29 at the National Synchrotron Light Source comes principally from the Offices of Biological and Environmental Research and of Basic Energy Sciences of the US Department of Energy, and from the National Center for Research Resources of the National Institutes of Health. The SGX Collaborative Access Team (SGX-CAT) beamline facilities at Sector 31 of the Advanced Photon Source were provided by SGX Pharmaceuticals, Inc., who constructed and operates the facility. Use of the Advanced Photon Source was supported by the U. S. Department of Energy, Office of Science, Office of Basic Energy Sciences, under Contract No. DE-AC02-06CH11357. Figures 1, 3B, 4A, and 5 were made using MacPyMOL [47]. Figure 4B was made using LIGPLOT [48]. G.A.P. was supported by a National Research Service Award (NIH F32 GM072326-01). W.J.L. was supported by National Institutes of Health MSTP grant GM07739 and by The W.M. Keck Foundation Medical Scientist Fellowship. This work was supported by National Institutes of Health grant GM53759 to S.A.D.

References

1. Murakami K, Darst SA. Bacterial RNA polymerases: the wholo story. Curr Opinion Struct Biol 2003;13:31–39.
2. Gross CA, Chan C, Dombroski A, Gruber T, Sharp M, Tupy J, Young B. The functional and regulatory roles of sigma factors in transcription. Cold Spring Harbor Symp Quant Biol 1998;63:141–155. [PubMed: 10384278]
3. Maeda H, Fujita N, Ishihama A. Competition among seven *Escherichia coli* sigma subunits: Relative binding affinities to the core RNA polymerase. Nucleic Acids Res 2000;28:3497–3503. [PubMed: 10982868]
4. Jishage M, Ishihama A. Regulation of RNA polymerase sigma subunit synthesis in *Escherichia coli*: Intracellular levels of sigma 70 and sigma 38. J Bacteriol 1995;177:6832–6835. [PubMed: 7592475]
5. Jishage M, Ishihama A. A stationary phase protein in *Escherichia coli* with binding activity to the major sigma subunit of RNA polymerase. Proc Natl Acad Sci USA 1998;95:4953–4958. [PubMed: 9560209]
6. Jishage M, Ishihama A. Transcriptional organization and in vivo role of the *Escherichia coli rsd* gene, encoding the regulator of RNA polymerase sigma D. J Bacteriol 1999;181:3768–3776. [PubMed: 10368152]
7. Jishage M, Kvint K, Shingler V, Nystrom T. Regulation of sigma factor competition by the alarmone ppGpp. Genes & Development 2002;16:1260–1270. [PubMed: 12023304]
8. Laurie AD, Bernardo LM, Sze CC, Skarfstad E, Szalewska-Palasz A, Nystrom T, Shingler V. The role of the alarmone (p)ppGpp in sigma N competition for core RNA polymerase. J Biol Chem 2003;278:1494–1503. [PubMed: 12421818]
9. Mitchell JE, Oshima T, Piper SE, Webster CL, Westblade LF, Karimova G, Ladant D, Kolb A, Hobman JL, Busby SJW, Lee DJ. The *Escherichia coli* regulator of sigma 70 protein, Rsd, can up-regulate some stress-dependent promoters by sequestering sigma 70. J Bacteriol 2007;189:3489–3495. [PubMed: 17351046]
10. Westblade LF, Ilag LL, Powell AK, Kolb A, Robinson CV, Busby SJW. Studies of the *Escherichia coli* Rsd-sigma 70 complex. J Mol Biol 2004;335:685–692. [PubMed: 14687566]
11. Dove SL, Hochschild A. Bacterial two-hybrid analysis of interactions between region 4 of the sigma 70 subunit of RNA polymerase and transcriptional regulators Rsd from *Escherichia coli* and AlgQ from *Pseudomonas aeruginosa*. J Bacteriol 2001;183:6413–6421. [PubMed: 11591686]
12. Jishage M, Dasgupta D, Ishihama A. Mapping of the Rsd contact site on the sigma 70 subunit of *Escherichia coli* RNA polymerase. J Bacteriol 2001;183:2952–2956. [PubMed: 11292818]
13. Campbell EA, Muzzin O, Chlenov M, Sun JL, Olson CA, Weinman O, Trester-Zedlitz ML, Darst SA. Structure of the bacterial RNA polymerase promoter specificity sigma factor. Mol Cell 2002;9:527–539. [PubMed: 11931761]
14. Geszvain K, Gruber TM, Mooney RA, Gross CA, Landick R. A hydrophobic patch on the flap-tip helix of *E. coli* RNA polymerase mediates sigma 70 region 4 function. J Mol Biol 2004;343:569–587. [PubMed: 15465046]

15. Kuznedelov K, Minakhin L, Niedziela-Majka A, Dove SL, Rogulja D, Nickels BE, Hochschild A, Heyduk T, Severinov K. A role for interaction of the RNA polymerase flap domain with the sigma subunit in promoter recognition. Science 2002;295:855–857. [PubMed: 11823642]

16. Murakami K, Masuda S, Darst SA. Structural basis of transcription initiation: RNA polymerase holoenzyme at 4 Å resolution. Science 2002;296:1280–1284. [PubMed: 12016306]

17. Vassylyev DG, Sekine S, Laptenko O, Lee J, Vassylyeva MN, Borukhov S, Yokoyama S. Crystal structure of a bacterial RNA polymerase holoenzyme at 2.6 Å resolution. Nature 2002;417:712–719. [PubMed: 12000971]

18. Ambrosi C, Tiburzi F, Imperi F, Putignani L, Visca P. Involvement of AlgQ in transcriptional regulation of pyoverdine genes in *Pseudomonas aeruginosa* PAO1. J Bacteriol 2005;187:5097–5107. [PubMed: 16030202]

19. Deretic K, Konyecsni WM. Control of mucoidy in *Pseudomonas aeruginosa*: Transcriptional regulation of *algR* and identification of the second regulatory gene, *algQ*. J Bacteriol 1989;171:3680–3688. [PubMed: 2544550]

20. Kato JL, Chiu L, Kitano K, DeVault JD, Kimbara K, Chakrabarty AM, Misra TK. Nucleotide sequence of a regulatory region controlling alginate synthesis in *Pseudomonas aeruginosa*: Characterization of the *algR2* gene. Gene 1989;84:31–38. [PubMed: 2514124]

21. Cacalano G, Kays M, Saiman L, Prince A. Production of the *Pseudomonas aeruginosa* neuraminidase is increased under hyperosmolar conditions and is regulated by genes involved in alginate expression. J Clin Invest 1992;89:1866–1874. [PubMed: 1601994]

22. Schlictman D, Kubo M, Shankar S, Chakrabarty AM. Regulation of nucleoside diphosphate kinase and secretable virulence factors in *Pseudomonas aeruginosa*: Roles of *algR2* and *algH*. J Bacteriol 1995;177:2469–2474. [PubMed: 7730279]

23. Severinova E, Severinov K, Fenyö D, Marr M, Brody EN, Roberts JW, Chait BT, Darst SA. Domain organization of the *Escherichia coli* RNA polymerase sigma 70 subunit. J Mol Biol 1996;263:637–647. [PubMed: 8947564]

24. Hendrickson WA. Determination of macromolecular structures from anomalous diffraction of synchrotron radiation. Science 1991;254:51–58. [PubMed: 1925561]

25. Bakolitsa C, Cohen DM, Bankston LA, Bobkov AA, Cadwell GW, Jennings L, Critchley DR, Craig SW, Liddington RC. Structural basis for vinculin activation at sites of cell adhesion. Nature 2004;430:583–586. [PubMed: 15195105]

26. Murzin AG, Brenner SE, Hubbard T, Chothia C. SCOP: A structural classification of proteins database for the investigation of sequences and structures. J Mol Biol 1995;247:536–540. [PubMed: 7723011]

27. Campbell EA, Tupy JL, Gruber TM, Wang S, Sharp MM, Gross CA, Darst SA. Crystal structure of *Escherichia coli* sigma E with the cytoplasmic domain of its anti-sigma RseA. Mol Cell 2003;11:1067–1078. [PubMed: 12718891]

28. Sorenson MK, Ray SS, Darst SA. Crystal structure of the flagellar sigma/anti-sigma complex sigma 28/FlgM reveals an intact sigma factor in an inactive conformation. Mol Cell 2004;14:127–138. [PubMed: 15068809]

29. Lambert LJ, Wei Y, Schirf V, Demeler B, Werner MH. T4 AsiA blocks DNA recognition by remodeling sigma 70 region 4. EMBO J 2004;23:2952–292. [PubMed: 15257291]

30. Pineda M, Gregory BD, Szczypinski B, Baxter KR, Hochschild A, Miller ES, Hinton DM. A family of anti-sigma70 proteins in T4-type phages and bacteria that are similar to AsiA, a transcription inhibitor and co-activator of bacteriophage T4. J Mol Biol 2004;344:1183–1197. [PubMed: 15561138]

31. Urbauer JL, Simeonov MF, Urbauer RJ, Adelman K, Gilmore JM, Brody EN. Solution structure and stability of the anti-sigma factor AsiA: implications for novel functions. Proc Natl Acad Sci USA 2002;99:1831–1835. [PubMed: 11830637]

32. Sharp MM, Chan CL, Lu CZ, Marr MT, Nechaev S, Merritt EW, Severinov K, Roberts JW, Gross CA. The interface of sigma with core RNA polymerase is extensive, conserved, and functionally specialized. Genes Dev 1999;13:3015–3026. [PubMed: 10580008]

33. Gregory BD, Nickels BE, Garrity SJ, Severinova E, Minakhin L, Urbauer RJ, Urbauer JL, Heyduk T, Severinov K, Hochschild A. A regulator that inhibits transcription by targeting a intersubunit

interaction of the RNA polymerase holoenzyme. Proc Natl Acad Sci USA 2004;101:4554–4559. [PubMed: 15070756]

34. Siegele DA, Hu JC, Walter WA, Gross CA. Altered promoter recognition by mutant forms of the sigma 70 subunit of *Escherichia coli* RNA polymerase. J Mol Biol 1989;206:591–603. [PubMed: 2661828]
35. Gardella T, Moyle T, Susskind MM. A mutant *Escherichia coli* sigma 70 subunit of RNA polymerase with altered promoter specificity. J Mol Biol 1989;206:579–590. [PubMed: 2661827]
36. Gregory BD, Nickels BE, Darst SA, Hochschild A. An altered-specificity DNA-binding mutant of *Escherichia coli* sigma 70 facilitates the analysis of sigma 70 function *in vivo*. J Mol Biol 2005;56:1208–1219.
37. Arifuzzaman M, Maeda M, Itoh A, Nishikata K, Takit C, Saito R, Ara T, Nakahigashi K, Huang HC, Hirai A, Tsuzuki K, Nakamura S, Altaf-Ul-Amin M, Oshima T, Baba T, Yamamoto N, Kawamura T, Ioka-Nakamichi T, Kitagawa M, Tomita M, Kanaya S, Wada C, Mori H. Large-scale identification of protein-protein interactions of *Escherichia coli* K-12. Genome Res 2006;16:686–691. [PubMed: 16606699]
38. Ilag LL, Westblade LF, Deshayes C, Kolb A, Busby SJW, Robinson CV. Mass spectrometry of *Escherichia coli* RNA polymerase: Interactions of the core enzyme with sigma 70 and Rsd protein. Structure 2004;12:269–275. [PubMed: 14962387]
39. Campbell EA, Darst SA. The anti-sigma factor SpoIIAB forms a 2:1 complex with sigma F, contacting multiple conserved regions of the sigma factor. J Mol Biol 2000;300:17–28. [PubMed: 10864495]
40. Doublie S. Preparation of selenomethionyl proteins for phase determination. Methods Enzymol 1997;276:523–530. [PubMed: 9048379]
41. Weeks CM, Miller R. The design and implementation of SnB v2.0. J appl Crystallogr 1999;32:120–124.
42. de, La Fortelle E.; Irwin, JJ.; Bricogne, G. SHARP: A maximum-likelihood heavy-atom parameter refinement and phasing program for the MIR and MAD methods. In: Bourne, P.; Watenpaugh, K., editors. Crystallographic Computing. 7. 1997. p. 1-9.
43. Abrahams JP, Leslie AGW. Methods used in the structure determination of bovine mitochondrial F_1 ATPase. Acta crystallographica 1996;D52:30–42.
44. Jones TA, Zou J-Y, Cowan S, Kjeldgaard M. Improved methods for building protein models in electron denstiy maps and the location of errors in these models. Acta crystallographica 1991;A47:110–119. [PubMed: 2025413]
45. Adams PD, Pannu NS, Read RJ, Brunger AT. Cross-validated maximum likelihood enhances crystallographic simulated annealing refinement. Proc Natl Acad Sci USA 1997;94:5018–5023. [PubMed: 9144182]
46. Laskowski RA, MacArthur MW, Moss DS, Thornton JM. PROCHECK - A program to check the stereochemical quality of protein structures. J appl Crystallogr 1993;26:283–291.
47. DeLano, WL. The PyMOL molecular graphics system. 2002. http://www.pymol.org
48. Wallace AC, Laskowski RA, Thornton JM. LIGPLOT: A program to generate schematic diagrams of protein-ligand interactions. Protein Eng 1995;8:127–134. [PubMed: 7630882]

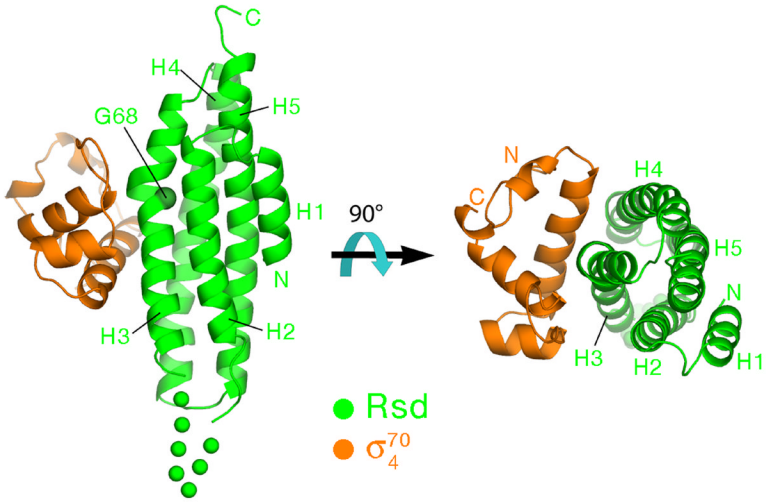

Figure 1. Structure of the σ^{70}_4/Rsd complex

Ribbon diagrams showing two orthogonal views of the complex, color-coded as shown. The α-helices of Rsd, H1–H5, are labeled. The α-carbon of Gly68 at the position of the kink in H3, is shown as a CPK sphere and labeled. A 7-residue disordered segment connecting H2 to H3 is represented by green dots.

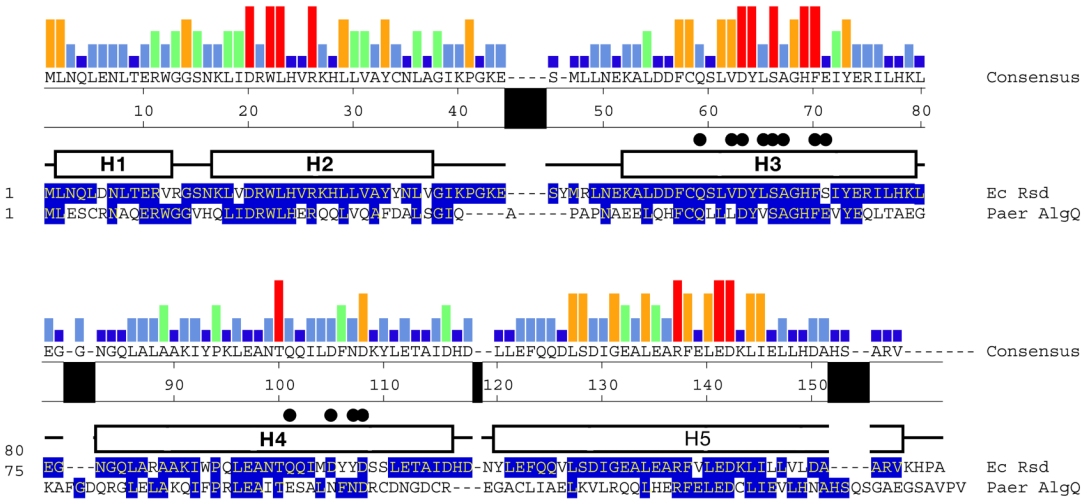

Figure 2. Sequence conservation among Rsd orthologs

The sequence on top shows the consensus sequence from an alignment of 113 Rsd orthologs (see supplemental information), while the histogram above it denotes the level of sequence conservation at each position (red bar, 100% conserved; dark blue bar, less than 20%). Shown are only two sequences from the full alignment, *E. coli* Rsd (top) and *Paer* AlgQ, represented in one-letter amino acid code and identified by the species at the right. The numbers at the beginning of each line indicate amino acid positions relative to the start of each protein sequence. The numbers at the top of the sequences indicate the amino acid position in *E. coli* Rsd. Amino acid identity with the consensus sequence is indicated by blue shading. The α-helices in the Rsd structure are indicated above the Rsd sequence as rectangles (labeled H1–H5), loops are indicated by a solid line. Rsd positions that contact σ^{70}_4 are denoted by black dots above the helices.

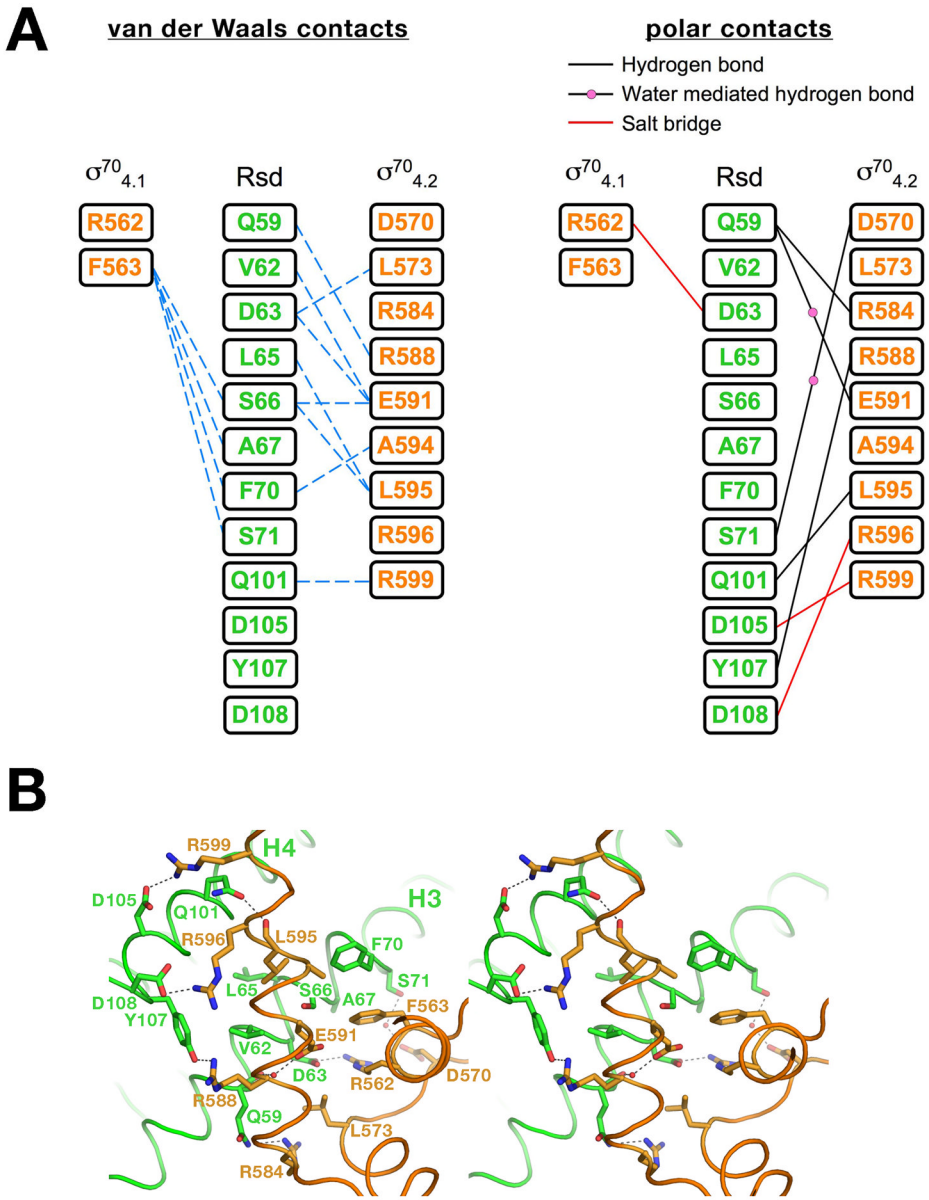

Figure 3. The σ^{70}_4/Rsd interactions

A) Schematic diagram denoting molecular interactions between Rsd and σ^{70}_4. Van der Waals interactions (<4 Å) are listed on the left, polar interactions (hydrogen bonds, salt bridges) are listed on the right.

B) Stereo view of the σ^{70}_4/Rsd interface. Protein α-carbon backbones are shown as worms, color-coded as in Figure 1. The two α-helices of Rsd harboring amino acid residues that interact with σ^{70}_4 (H3 and H4) are labeled. Amino acid side chains that participate in interprotein interactions are shown, with carbon atoms color-coded as the backbone worm, nitrogen atoms colored blue, and oxygen atoms colored red. Interprotein polar interactions (hydrogen bonds or salt bridges) are indicated by dashed lines.

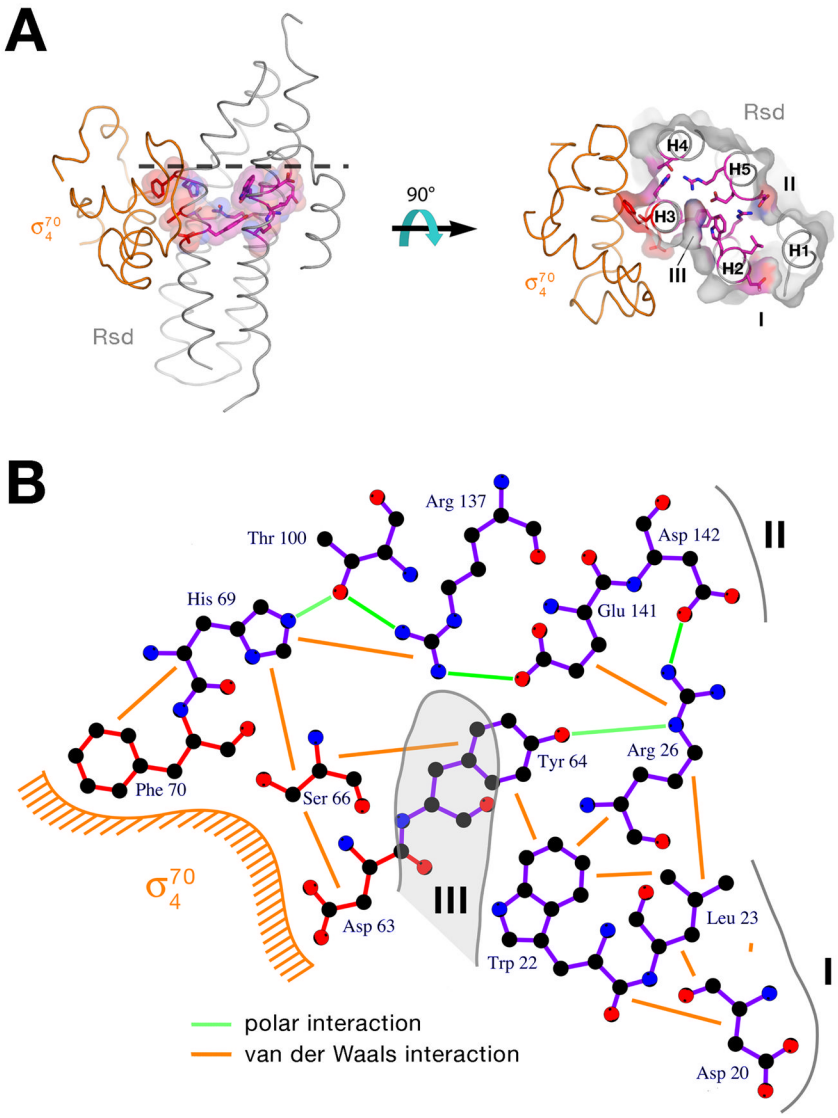

Figure 4. Interacting network of conserved residues in Rsd

A) Two orthogonal views of the σ^{70}_4/Rsd complex (similar views as Figure 1). The α-carbon backbones are shown as worms, with σ^{70}_4 colored orange, and Rsd colored grey. The side chains of the 13 absolutely conserved Rsd residues are shown (nitrogen, blue; oxygen, red), with carbon atoms colored magenta, except the three residues that interact directly with σ^{70}_4 (Asp63, Ser66, Phe70) are red. In the left view, transparent van der Waals surfaces for the conserved residues (color-coded as the atoms) is also shown, showing the continuous network through the middle of the Rsd structure. In the right view, the Rsd structure is shown as a cross-section, sliced at the level of the dashed line in the left view. On the right, the transparent molecular surface of Rsd is shown, colored grey except where the conserved residues are surface exposed. The Rsd helices (H1–H5), viewed mostly end-on, are labeled, as are the three cavities containing surface-exposed conserved residues (I, II, and III).

B) Schematic diagram showing the 13 conserved Rsd residues (bonds color-coded as in A, carbon atoms colored black) and illustrating the polar (hydrogen bonds or salt bridges, green lines) and van der Waals (< 4 Å, orange lines) interactions. The relative locations of σ^{70}_4, and cavities I, II, and II are indicated.

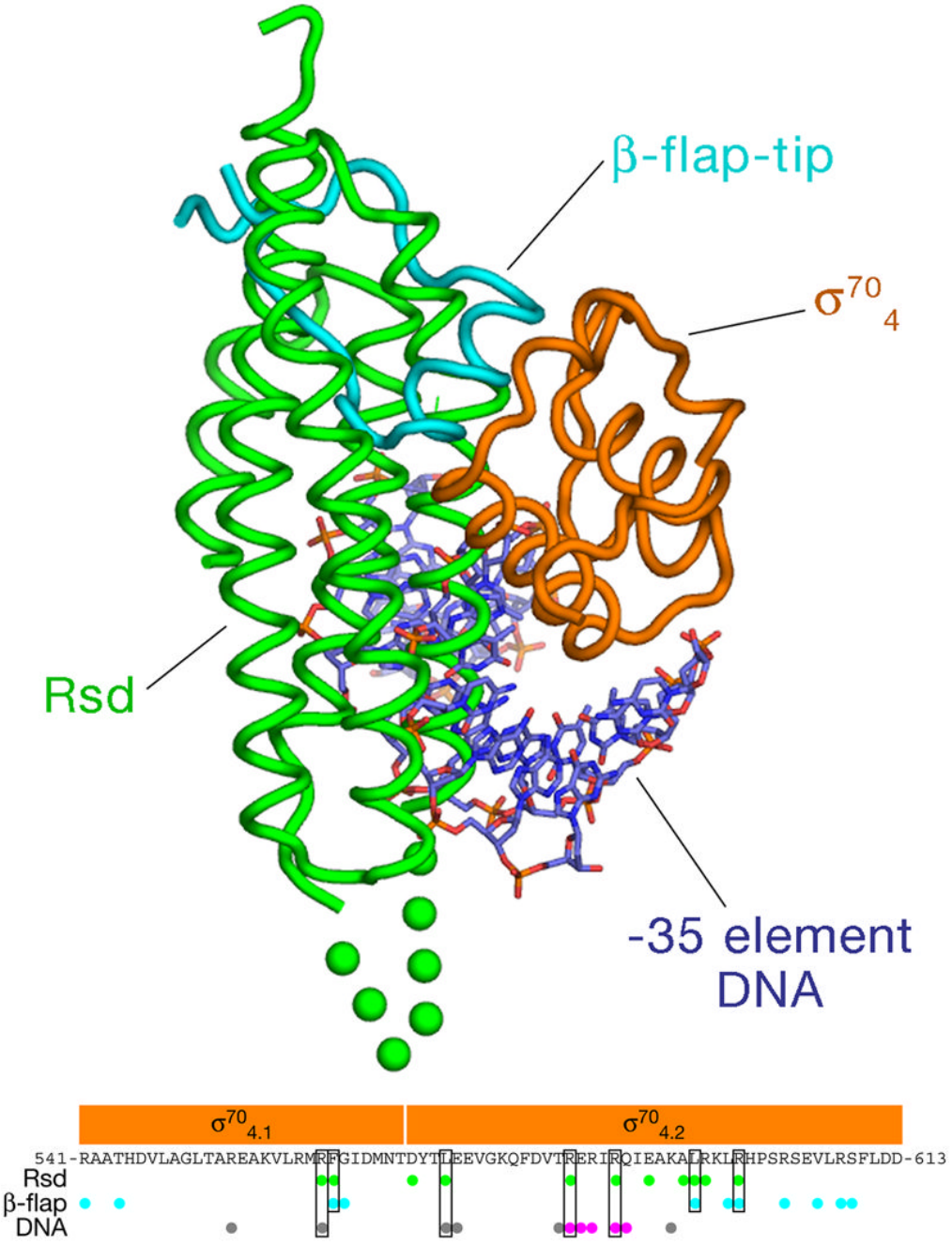

Figure 5. Rsd sterically occludes core RNAP and –35 element promoter DNA binding by σ^{70}_4

The σ^{70}_4/Rsd complex is shown with the α-carbon backbones as worms (Rsd, green; σ^{70}_4, orange). Superimposed is the position of the β-flap-tip (*T. aquaticus* RNAP β-subunit residues 759–788, corresponding to *E. coli* RNAP β-subunit residues 887–916), shown as a cyan backbone worm as it would be interacting with σ_4 in the context of the RNAP holoenzyme [17]. Also superimposed is the –35 element DNA as it would be interacting with σ4 13. Both the β-flap-tip and the –35 element sterically clash with Rsd. Below is a diagram schematically illustrating amino acid residues of σ4 that are involved in interactions with Rsd, the RNAP σ-subunit flap (Murakami et al., 2002; Vassylyev et al., 2002), and –35 element promoter DNA (Campbell et al., 2002). Shown in single-letter amino acid code is the sequence of *Ec*σ^{70}_4.

Conserved regions 4.1 and 4.2 are indicated above the sequence. Dots below the sequence mark σ4 residues involved in interactions with Rsd (green dots), the RNAP β-flap (cyan dots), or –35 element promoter DNA (grey dots, DNA phosphate backbone; magenta dots, sequence-specific interactions). Residues that interact with Rsd and are also involved in interactions with the β-flap or –35 element DNA are boxed.

Table 1

Crystallographic Analysis

Diffraction Data								
Data Set	**Beamline**	**Wavelength (Å)**	**Resolution (Å)**	**No. of Reflections (tot./unique)**	**Completeness (%) (tot./last shell)**	***I*/σ(*I*) (tot./last shell)**	**R_{sym} [c] (%) (tot./last shell)**	**No. of Sites**
Native	NSLS[a] X29	1.1	50–2.6 (2.7–2.6)	144,443/10,405	99.1 (98.8)	17.2 (2.2)	8 (48.6)	
SeMet1(λ1)	APS SGX[b] 31-ID-D	0.9793 (peak)	20–2.9 (3.0-2.9)	117,509/7,527	98.2 (87.1)	8.5 (1.3)	11.7 (44.7)	4
SeMet1(λ1)	APS SGX[b] 31-ID-D	0.9641 (remote)	20–3.1 (3.21-3.1)	132,551/6,187	99.5 (97.5)	7.7 (1.4)	13.5 (52.1)	4
Crystal space group, $P6_422$; unit cell, a = b = 84.111 Å, c = 84.219 Å; Figure of Meritd (30 - 2.9 Å resolution), 0.35								
Refinement (against Native data set)								
Resolution (Å)	50 – 2.6							
No. of solvent molecules	98							
R_{cryst}/R_{free} [e] (%)	24.0/27.3							
rmsd bond lengths	0.008 Å							
rmsd bond angles	1.328°							

[a] National Synchrotron Light Source, Brookhaven, NY;

[b] Advanced Photon Source-Structural GenomiX, Argonne, IL;

[c] $R_{sym} = \Sigma|I - \langle I \rangle|/\Sigma I$, where I is observed intensity and $\langle I \rangle$ is average intensity obtained from multiple observations of symmetry related reflections;

[d] Figure of merit calculated by SHARP (de la Fortelle et al. 1997);

[e] $R_{cryst} = \Sigma||F_{observed}| - |F_{calculated}||/\Sigma|F_{observed}|$, $R_{free} = R_{cryst}$ calculated using 5% random data omitted from the refinement.